Article ID: 1007-4627(2013) 03-0221-10

Large Mass Transfer Reaction and Production of Neutron Rich Superheavy Nuclei

WU Xizhen[1]，ZHAO Kai[1]，LI Zhuxia[1]，WANG Ning[2]，
TIAN Junlong[3]，ZHANG Yingxun[1]

(*1. China Institute of Atomic Energy, Beijing 102413, China*；
2. Guangxi Normal University, Guilin 541004, Guangxi, China；
3. Anyang Normal University, Anyang 455000, Henan, China)

Abstract：For elements with $Z > 100$ only neutron deficient isotopes have been synthesized so far. The "north-east area" of the nuclear map can be reached neither in fusion-fission reactions nor in fragmentation processes. The large mass transfer reactions in near barrier collisions of heavy (U-like) ions seem to be the only reaction mechanism allowing us to produce neutron rich heavy nuclei including those located at the superheavy(SH) island of stability and unexplored area of heavy neutron-rich nuclides. This study is extremely important for nuclear astrophysical investigations and, in particular, for the understanding of the *r* process. In this paper within the Improved Quantum Molecular Dynamics (ImQMD) model combining with the statistical-evaporation model, the large mass transfer reactions, like ^{238}U+^{238}U have been studied. The charge and mass distributions of transiently formed primary fragments are investigated within the ImQMD model and de-excitation processes of those primary fragments are described by the statistical decay model. The mass distribution of the final products in ^{238}U+^{238}U collisions is obtained and compared with the recent experimental data. Through compared the formation cross sections of transfermium element 106 by three reactions of ^{136}Xe+^{248}Cm, ^{48}Ca+^{248}Cm and ^{238}U+^{248}Cm, it is explored that the large mass transfer reactions, like U+U are very benefit for the production of SH nuclei.

Key words: large mass transfer reaction; superheavy nuclei; U+U reaction; heavy neutron-rich nuclei

CLC number: O571.6 **Document code:** A **DOI:** 10.11804/NuclPhysRev.30.03.221

1 Introduction

It is well known that due to the "curvature" of the β stability line in fusion reactions of stable nuclei we may produce only proton-rich isotopes of heavy elements. So up to now all synthesized superheavy (SH) elements are only neutron deficient isotopes, which are all short life time and far from the stability island. In the "cold" fusion reactions based on the closed-shell target nuclei, lead and bismuth, proton-rich SH elements up to $Z = 113$ have been produced[1−2]. The "world" record of 0.03 pb in the production cross section of the 113 element has been obtained within more half-year irradiation of ^{209}Bi target with ^{70}Zn beam. Further advance in this direction seems to be very difficult. In the "hot" fusion the heaviest available targets of berkelium ($Z = 97$) and californium ($Z = 98$) have been used to produce the elements 117 and 118[3−4]. To get SH elements with $Z > 118$ in fusion reactions, one should proceed with projectiles heavier than ^{48}Ca . The nearest to ^{48}Ca projectile, ^{50}Ti, may be the most promi-sing one for further synthesis of SH nuclei. The use of the titanium beam instead of ^{48}Ca decreases the yield of SH nuclei mainly due to a worse fusion probability. The calculated excitation functions for the synthesis of SH elements

Received date: 29 Oct. 2012； **Revised date:** 25 Mar. 2013

Foundation item: National Natural Science Foundation of China(11005022, 11005155, 10875031, 10975095, 10905021, 91126010, 11005003，U1230127); Defense Industrial Technology Development Program(B0120110034)

Biography: WU Xizhen, (1940–), male，Hebei Dongguang, Professor，working on field of nuclear fission, heavy ion reactions and transport theory；E-mail: lizwux@ciae.ac.cn.

119 and 120 in the fusion reactions of ^{50}Ti with ^{249}Bk and ^{249}Cf targets reach maximal values of about 0.05 pb in 3n and 4n evaporation channels[5]. However, as mentioned above, due to the bending of the stability line forward the neutron axis, in this fusion reaction only proton-rich SH nuclei with a short half-life can be produced, which locate far from the "island of stability" (see Fig. 1). Note that the half-lives of the isotopes of 120 element synthesized in the titanium induced fusion reaction are already very close to the critical value of 1 μs needed to pass through the separator up to the focal plane detector. The next elements ($Z > 120$) being synthesized in such a way might be beyond this natural limit for this detection. Thus, further studies of SH elements are connected with the production of neutron-enriched longer living isotopes of SH nuclei. There are three possibilities for production of such nuclei. These are the large mass transfer reactions, fusion reactions with extremely neutron-rich radioactive nuclei and rapid neutron capture process. Today the two last methods look unrealizable because of low intensity of radioactive beams and low neutron fluxes in existing nuclear reactors. The large mass transfer reaction is the only practicable way in the present time.

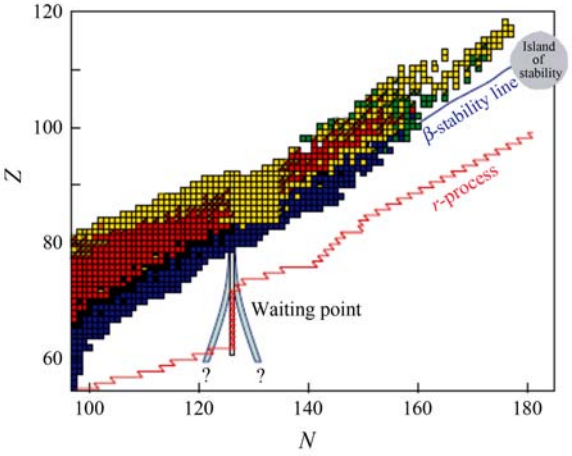

Fig. 1 (color online) Top part of the nuclear map. The *r*-process path and the island stability are skown schematically.

On the other hand, we know that there is almost no information about neutron-rich isotopes of heavy elements located in the whole 'northeast part of the nuclear map'. This unexplored area of heavy neutron-rich nuclei is extremely important for nuclear astrophysics investigations, in particular, for the understanding of the *r*-process of astrophysical nucleogenesis. The origin of heavy elements from iron to uranium remains one of the great unanswered questions of modern physics and it is likely to remain a hot research topic for years to come. The *r*-process path is located just in the region of unknown heavy nuclei with the large neutron excess (see Fig. 1). The isotopes with extremely neutron-to-proton ratios in the mass region $A = 80 \sim 140$ are successfully produced, separated and studied in fission processes of actinide nuclei, whereas the neutron-rich nuclei with $Z > 60$ cannot be formed neither in fission nor in fusion reactions. This area of the nuclear map remains blank for many years. Therefore, a special attention is paid to the large mass transfer reaction.

The main approaches to study the large mass transfer reactions theoretically are as follows:

(1) The microscopic transport theory , i.e., the Improved Quantum Molecular Dynamics (ImQMD) model[6]; (2) The time-dependent Hartree-Fock (TDHF) theory[7]; (3) The coupled Langevin-type equations[8]; (4) The dinucleus system approach[9].

Among those approaches, the TDHF theory can describe the collision process between heavy (actinide) nuclei microscopically, but seems to be difficult to give the mass (charge) distributions of the large mass transfer reactions. The coupled Langevin-type equations are used to describe the large mass transfer reactions macroscopically. They also have some limitations, for example, the large number of collective degrees of freedom have to be involved for describing the complicated process of the large mass transfer reactions; there are the difficulties of calculation of multi-dimensional potential surfaces and the large uncertainty of mass parameters and viscosity tensor. On the contrary, the ImQMD model is a microscopic model, which considers each of nucleons as a wave pocket. A system size dependent wave pocket width is introduced to consider the evolution of the wave pocket width during the collision process between two heavy nuclei. The surface and surface symmetry energy terms are introduced in the potential energy density functional. An approximate treatment of antisymmetrization, namely, the phase space occupation constraint is adopted and a part of structure effect of initial nuclei is also taken into account. So the dissipation, diffusion and correlation are all included in the model without introducing any freely adjusting parameters.

In this work we briefly discuss the behaviors of the

giant composite systems formed in two heavy nuclear collisions and the primary mass (charge) distributions after breakup of the giant composite systems by the ImQMD model; Considering the extreme complexity of the reaction process and the need to reduce computation time, we describe the final mass (charge) distributions by a two-step model, that is the dynamic reaction process described by the ImQMD model followed by a statistical decay process, which is described by a statistical decay model.

2 Primary mass distributions after breakup of the composite system

In this approach, the first step describes the formation and re-separation process of the transiently formed composite systems of ^{238}U+U using the ImQMD model. It gives the full information of each proton and neutron as well as all re-separation primary fragments at any reaction time. The second step is devoted to describing the decay of the primary fragments using the computer code HIVAP incorporating a three-Gaussian model to describe the mass distribution of fission fragments. Finally, the mass distribution of the products is obtained.

Now we first study the primary mass distribution after breakup of the giant composite systems. The charge, mass, and excitation energy distributions as well as the angular distribution of primary fragments are obtained by the ImQMD model calculations. The double differential cross section of a primary fragment with charge Z, mass A, excitation energy E, and scattering angle θ is given by

$$\frac{\mathrm{d}^2\sigma_{\mathrm{pri}}(Z,A,E,\theta)}{\mathrm{d}\theta\mathrm{d}E} = \int_0^{b_{\max}} 2\pi b f(Z,A,E,\theta,b)\mathrm{d}b = \sum_{i=0}^{i_{\max}} 2\pi b_i f_i(Z,A,E,\theta,b_i)\Delta b \,,$$

where $f(A,\ Z,\ E,\ \theta,\ b)$ is the probability of producing the primary fragments with charge Z, mass A, excitation energy E, and scattering angle θ under impact parameter b. The maximum impact parameter $b_{\max}$ is taken to be 14 fm because there is no inelastic scattering when $b > 14$ fm. The double differential cross section for primary fragments will be used as input in the second step for the calculations of final products to compare with the measurement. Let us first study the charge and mass distribution of primary fragments, which is the integration of double differential cross sections. In Fig. 2 we show the charge distributions for ^{238}U+^{238}U at 830 MeV and b=1 fm at different reaction times t = 1 000, 1 300 and 1 600 fm/c. From the figure, we can see that at t = 1 000 fm/c (solid squares) the systems with $Z \sim 184$ are dominant, and the number of fragments is very small. With time up to 1 300 fm/c (open circles), the number of systems with $Z \sim 184$ decreases to the same order of magnitude as that of fragments, and at t = 1 600 fm/c (solid triangles) the fragments are dominant, and only very few systems with $Z \sim 184$ survive.

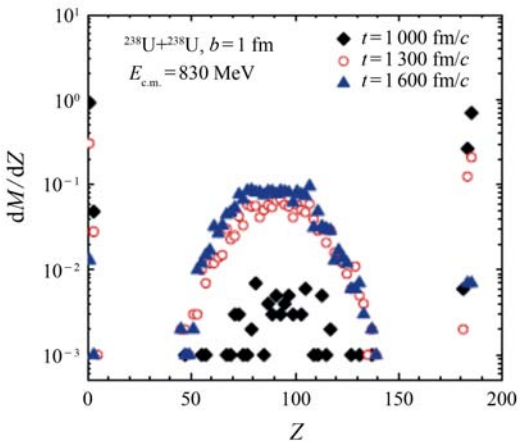

Fig. 2　(color online) Charge distributions of ^{238}U+^{238}U at the c.m energy 830 MeV and b = 1 fm, at the reaction times of 1 000, 1 300 and 1 600 fm/c.

Figs. 3 shows the charge and mass distribution of primary fragments at 3 000 fm/c for ^{238}U+^{238}U at 7.0 AMeV, respectively. A sharp peak indicates that uranium is present in both figures. The primary fragments on the left-hand side of the sharp peak stem from the re-separation of the composite system and fast fission products of actinide and transactinide fragments. The products on the right-hand side of the sharp peak correspond to transuranic nuclei. The mass distributions of primary fragments at 3 000 fm/c for different impact parameters are calculated to clarify the origin of the fragments with different mass regions. The results are shown in Fig. 4. Figs 4(a) $\sim$ 4(d) are for the impact parameters of 0$\sim$4, 5$\sim$7, 8$\sim$10, and 11$\sim$14 fm, respectively. In central collisions [see Fig. 4(a)], the mass number distribution of primary fragments extends to A = 320 with a big asymmetric hump around $A = 200 \sim 260$, which means that a large mass transfer between two uranium nuclei occurs in central collisions. In semicentral collisions [Fig. 4(b)], the mass distribution becomes narrower with a much shorter tail on the right-hand side. Two peaks appear in the mass distribution, with the larger one corresponding to uranium and the smaller one originating

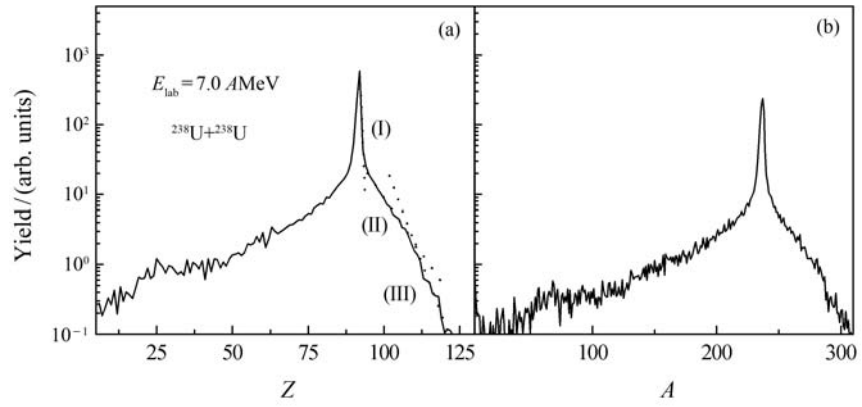

Fig. 3 (a) The charge and (b) the mass distribution of the primary fragments of ^{238}U+^{238}U at 7.0 *A*MeV.

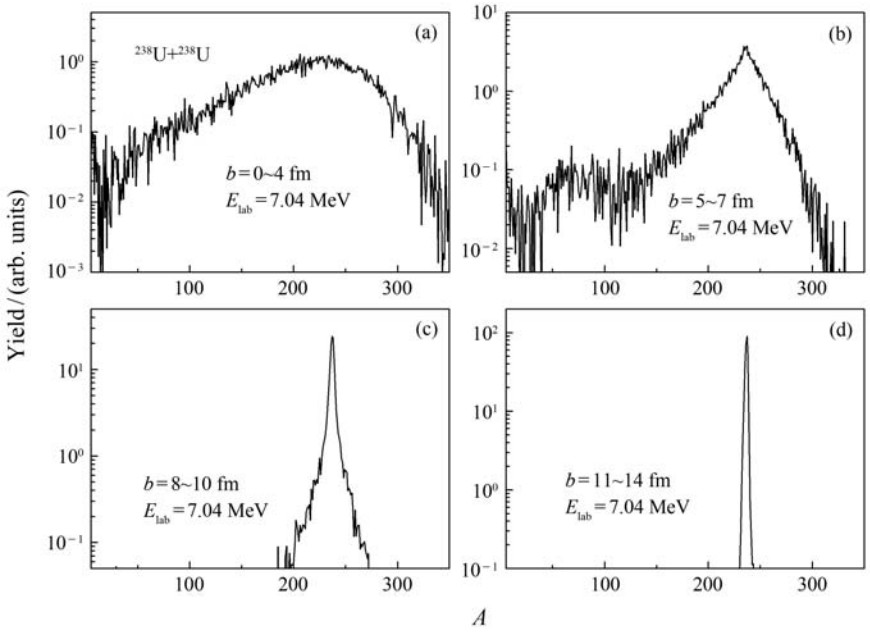

Fig. 4 The mass distributions of the primary fragments for ^{238}U+^{238}U at 7.0 *A*MeV at different impact parameter regions.

from ternary-like fission (or occasionally from quaternary fission) events in the reaction ^{238}U+^{238}U. Here, the shell effect may play an important role in the above and near barrier collisions. It may occur if one of the colliding nucleus ^{238}U gives away nucleons approaching the doubly magic ^{208}Pb nucleus; whereas another ^{238}U can accept these nucleons becoming SH (transuranic) nuclei. A little part of those SH nuclei make de-excitation and survive, but most part of them have possibility that they split again into ^{208}Pb nuclei and another fragments with mass around $40 \sim 60$. This leads to the small peak in Fig. 4(b). It should be indicated that the shell effect leads to enhanced production yield of SH nuclei in the multi-nucleon transfer reaction compared to the fusion reaction. Therefore, for production of neutron-rich or very heavy SH nuclei the multi-nucleon transfer reaction may be a more possible way compared to the complete fusion reaction. For the peripheral collisions [Figs. 4(c) and 4(d)], the mass distribution of primary fragments shows a symmetric peak with very little variance. The reaction mechanism for peripheral reactions is inelastic or elastic scattering between two uranium nuclei. To understand the reaction mechanism and the mass distribution of fragments evolving with impact parameters shown in Fig. 4, we present the average lifetime of a transiently formed composite system for ^{238}U+^{238}U at 7 *A*MeV as a function of impact parameter in Fig. 5. From this figure, one can see that the lifetime of the composite system increases as impact parameter decreases. In central collisions, two uranium nuclei have a longer interaction time, with a stronger dissipation of collective motion, and thus

there is stronger mass transfer between them than with larger impact parameter cases. Therefore, the SH (transuranic) primary fragments mainly come from the central and semi-central collisions.

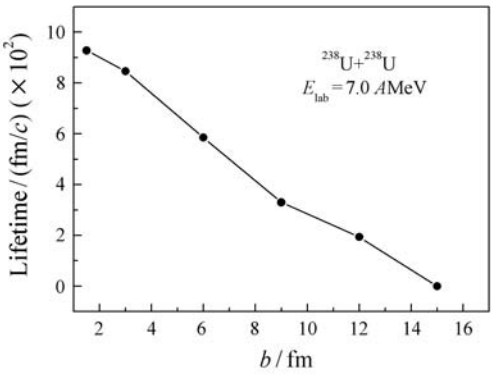

Fig. 5　The impact-parameter dependence of the average lifetime for the composite system of ^{238}U+^{238}U at 7 *A*MeV.

In order to manifest above large mass transfer reaction to be very benefit for the production of neutron-rich transfermium isotopes, we compare three reactions of ^{238}U, ^{136}Xe, and ^{48}Ca with curium target. In Fig. 6 shows the charge and mass distributions of heavy primary reaction fragments are shown for near barrier collisions of ^{238}U, ^{136}Xe, and ^{48}Ca with curium target[10]. The "lead shoulder" manifests itself in all these reactions. However, for ^{136}Xe+^{248}Cm and ^{48}Ca+^{248}Cm collisions it corresponds to the usual (symmetrizing) quasifission process in which nucleons are transferred mainly from the heavy target (here it is ^{248}Cm) to the lighter projectile. This is a well-studied process both experimentally[11] and theoretically[12]. It is caused just by the shell effects leading to the deep lead valley on the multidimensional potential energy surface which regulates the dynamics of the heavy nuclear system at low-excitation energies. Contrary to this ordinary quasifission phenomena, for the ^{238}U+^{248}Cm collisions we may expect an inverse process in which nucleons are predominantly transferred from the lighter partner (here it is uranium) to the heavy one (i.e., U transforms to Pb and Cm to 106 element). In this case, besides the lead shoulder in the mass and charge distributions of the reaction fragments, there is also a pronounced shoulder in the region of SH nuclei (see Fig. 6). As a result, the cross sections for formation of new neutron-rich isotopes of transfermium elements in transfer reactions with ^{248}Cm target are larger by several orders of magnitude as compared with the reactions of ^{136}Xe+^{248}Cm and ^{48}Ca+^{248}Cm. These results indicate that the large mass transfer reaction is very benefit for the production of transfermium elements (SH elements).

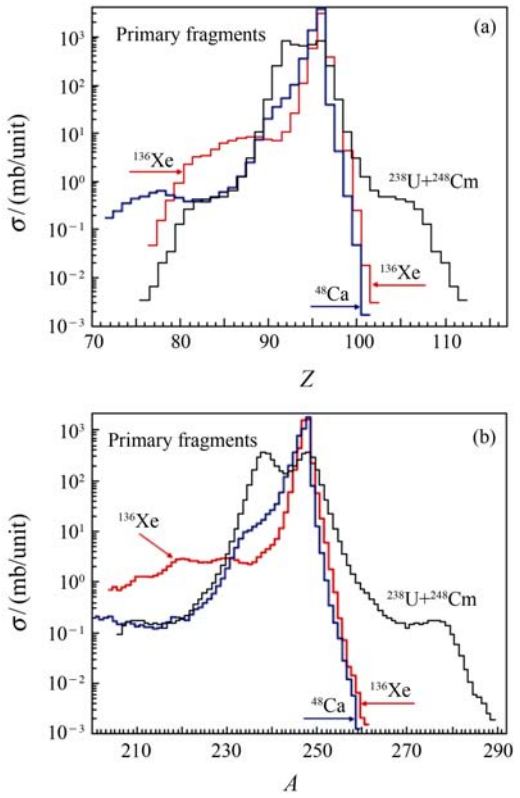

Fig. 6　(color online) Charge (a) and mass (b) distributions of heavy primary reaction fragments formed in collisions of ^{238}U, ^{136}Xe, and ^{48}Ca with ^{248}Cm target at $E_{\mathrm{c.m.}}$ = 750, 500, and 220 MeV correspondingly.

3　Mass distribution of final products

From the ImQMD model calculation, we obtain the distributions of charges, masses, and excitation energies for all primary fragments produced in ^{238}U+^{238}U collisions. These primary fragments will de-excite through the emission of light particles or γ rays or through fission. The decay process and final products are described by the statistical evaporation model (HIVAP code) incorporating the three-Gaussian fission model. In HIVAP, the survival probability of an excited primary fragment is given by a subsequent de-excitation process, leading to a given final evaporation residue nucleus in its ground state. Successive stages of a subsequent de-excitation process for primary fragments with mass A, charge Z, and excitation energy E are determined by branching ratios expressed

by relative partial decay widths for all possible decay modes, $\Gamma_i(A,Z,E)/\Gamma_{tot}(A,Z,E)$, where i=n, p, d, α, etc. and $\Gamma_{tot}(A,Z,E)$ is the sum of all particle decay widths $\Gamma_i(A,Z,E)$ and the fission width $\Gamma_f(A,Z,E)$. All partial widths for emission of light particles and fission for excited nuclei are calculated by the HIVAP code. The excited actinide and transactinide nuclei in primary fragments and those produced in the de-excitation process undergo fission. The production probability of a fission fragment with mass number A_1 is calculated as follows:

$$W_f(A_1)=\sum_{A,Z,E}\frac{\Gamma_f(A,Z,E)}{\Gamma_{tot}(A,Z,E)}P(A_1,A,Z,E)\ .$$

Here, $P(A_1,A,Z,E)$ is the probability of production of a fragment with mass number A_1 from fission of the excited nucleus with mass A, charge Z, and excitation energy E. $P(A_1,A,Z,E)$ is calculated on the basis of an empirical three-Gaussian model and is given as

$$P(A_1,A,Z,E)=\sum_{i=1}^{3}g^{(j)}(A_1,A,Z,E)$$

and

$$g^{(j)}(A_1,A,Z,E)=\frac{P^{(j)}(A,Z,E)}{\sqrt{2\pi}\sigma^{(j)}(A,Z,E)}\times \exp\left\{-\frac{\left[A_1-A^{(j)}(A,Z,E)\right]^2}{2\left[\sigma^{(j)}(A,Z,E)\right]^2}\right\},\quad j=1,2,3\ .$$

Here, the Gaussian distribution $g^{(j)}(A_1,A,Z,E)$ represents one of the components of the mass distribution of fission. Among them, $g^{(1)}(A_1,A,Z,E)$ and $g^{(2)}(A_1,A,Z,E)$ describe the asymmetric component of the mass distribution, and $g^{(3)}(A_1,A,Z,E)$ describes the symmetric component. $P^{(j)}(A,Z,E)$, $\sigma^{(j)}(A,Z,E)$, and $A^{(j)}(A,Z,E)$ are the parameters for three-Gaussian distributions, which are functions of the mass number A, charge Z, and excitation energy E of the fissile nucleus. $P^{(j)}(A,Z,E)$ and $A^{(j)}(A,Z,E)$ exhibit the following relationships:

$$\begin{aligned}P^{(1)}(A,Z,E)&=[1-P^{(3)}(A,Z,E)]\eta\\ P^{(2)}(A,Z,E)&=[1-P^{(3)}(A,Z,E)](1-\eta)\\ A^{(1)}(A,Z,E)&+A^{(2)}(A,Z,E)=A\\ A^{(3)}(A,Z,E)&=\frac{A}{2}\end{aligned}$$

Thus, only six parameters of $P^{(3)}(A,Z,E)$, η, $A^{(1)}(A,Z,E)$ and $\sigma^{(j)}(A,Z,E)(j=1,2,3)$ are independent, which need to be fixed according to the available experimental data of fission mass distributions in actinide and transactinide nuclei. For fitting the parameters in the three-Gaussian empirical formula, we collected as many available experimental data of fission mass distributions[13−17] as possible. In cases where experimental data are lacking, interpolation or extrapolation is employed. For ^{238}U, data for the mass distributions of fission fragments at different energies are available, so we can obtain the energy dependence of mass distribution of fission fragments through interpolation. However, these data are not available for other fissile nuclei. For these nuclei, we suppose that they have an energy dependence behavior similar to those of ^{238}U for lack of the corresponding theoretical study for these nuclei. This, of course, will introduce a considerable approximation. However, in the reaction considered in this work, the fission for excited ^{238}U is the most important among all fissile nuclei, and we expect that the approximation introduced in the energy dependence of the mass distribution of fission fragments will not severely damage the accuracy of the final results. In Figs. 7∼8, we show some examples of calculated mass distributions of fission for different nuclei and for different excitation energies, and we compare these with experimental data. The curves and dots denote calculated results and data, respectively. From those figures, we can see that the empirical formula seems to successfully reproduce the available experimental data and can be used to calculate the mass distributions of actinide and transactinide fragments. On the basis of this model, the mass distribution of final products for ^{238}U+^{238}U at an incident energy of 7.0 *A*MeV can be calculated. In Fig. 9, we show the calculated results of final products at four impact parameter regions of $0\sim4$, $5\sim7$, $8\sim10$, and $11\sim14$ fm. For central collisions [see Fig. 9(a)], the reseparation primary fragments of ^{238}U+^{238}U systems carry high excitation energies, with the majority of them undergoing symmetric fission and thus a single hump of mass yield is found at around mass number 120. The rest of the fragments that do not undergo fission will exhibit evaporation of particles, and their residues finally form a shoulder in the mass distribution around Pb, which is due to strong shell effects for those nuclei around Pb. The yields for transuranic fragments decrease rapidly as mass increases, which is due to the high excitation energy of primary fragments in central collisions, as seen from Fig. 9(a). Here, we should mention that the yields of the tran-

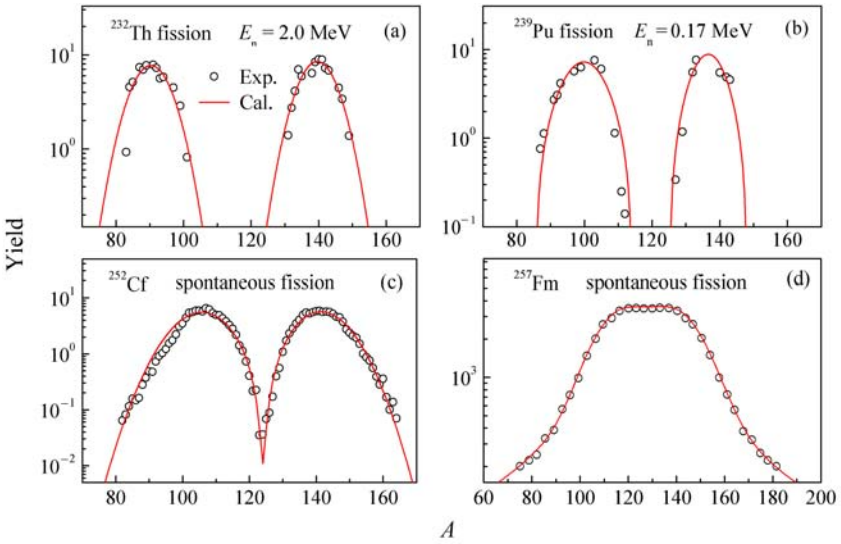

Fig. 7　(color online) The mass distributions of fission products for ^{232}Th, ^{239}Pu, ^{252}Cf, and ^{257}Fm. The experimental data are taken from Refs. [17-20].

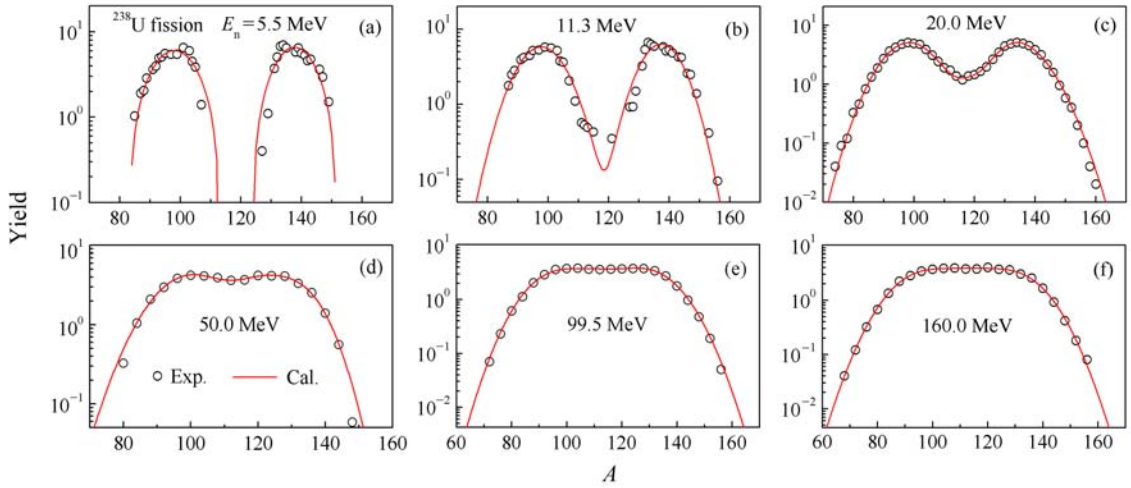

Fig. 8　(color online) The mass distributions of fission products for ^{238}U at different excitation energies. The experimental data are taken from Ref. [7].

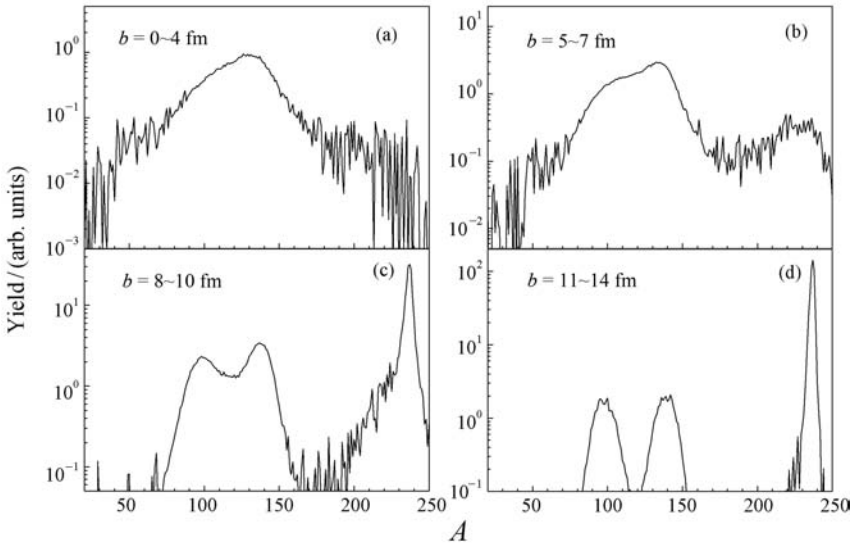

Fig. 9　The mass distribution of the products in ^{238}U+^{238}U at different impact parameter regions.

suranic nuclei are not very certain because the fission barrier and the fission width for SH nuclei and the transuranic nuclei are largely uncertain. For semicentral collisions, that is, in the impact parameter region of $5 \sim 7$ fm [see Fig. 9(b)], the excitation energies carried by primary fragments are much less than those in the central collisions, so a broad hump appears in the mass number region of $80 \leqslant A \leqslant 170$, which is the superposition of symmetric and asymmetric fission. Another small hump centered at uranium ($A \approx 230$) appears. The shallow valley between two humps means that the yields of nuclei around Pb are still considerable. Here, we notice that the yields of transuranic nuclei are relatively high compared with those in central collisions, which is due to the excitation energies of primary fragments being much lower than those in central collisions. For peripheral collisions [see Figs. 9(c) and 9(d)], elastic or inelastic scattering plays a dominant role and the behavior of low-energy fission of actinide nuclei is shown. The small shoulder around Pb seems to appear for impact parameters $b = 8 \sim 10$ fm [see Fig. 9(c)].

To perform a comparison with the experimental measurement, we must select a scattering angle to fit the angle cut in the experimental data, that is, only fragments with scattering angles of $56° \leqslant \theta \leqslant 84°$ and $96° \leqslant \theta \leqslant 124°$ in the center-of-mass frame are selected[21]. In the calculations, we assume that the scattering angle of the residue of the primary fragment that exhibits emission of light charged particles is the same as that of the fragment itself. This assumption is reasonable since the mass of the residue is much larger than that of the emitted light particles. For fragments from fission, we assume that the outgoing angle of one fragment is randomly distributed in the rest frame of the fissioning nucleus, and the outgoing angle of the other one is then obtained by momentum conservation. Finally, we obtain the mass distribution of the final products with the same scattering angle as that cut in the experiment. The results are shown by open triangles in Fig. 10. The experimental mass spectra from Ref. [21] are also indicated by solid squares, open squares, solid circles, open circles, and solid triangles for incident energies of 6.09, 6.49, 6.91, 7.10, and 7.35 *A*MeV, respectively, in Fig. 10. From the figure, we find that the behavior of the calculated mass distribution at 7.0 *A*MeV is generally in agreement with the data at the incident energy 7.10 *A*MeV, except that the yields at the mass region from 170 to 210 are overestimated compared with the experimental data. The most important features of mass distribution are considered to be the following: (1) A dominant peak around uranium is observed, this can be attributed to the contribution of the reactions with large impact parameters; (2) A steep decreasing yield above U with increasing mass number appears. The products at this mass region stem from large mass transfer in small-impact-parameter reactions; (3) A small shoulder can be seen in the distribution of the products around Pb, compared with the products with a mass near and smaller than uranium for which the yields decrease exponentially as mass decreases. The appearance of the small shoulder is due to the very high fission barrier around Pb. The central and semicentral collisions, and even reactions with $b = 8 \sim 10$ fm, contribute to the shoulder in the region

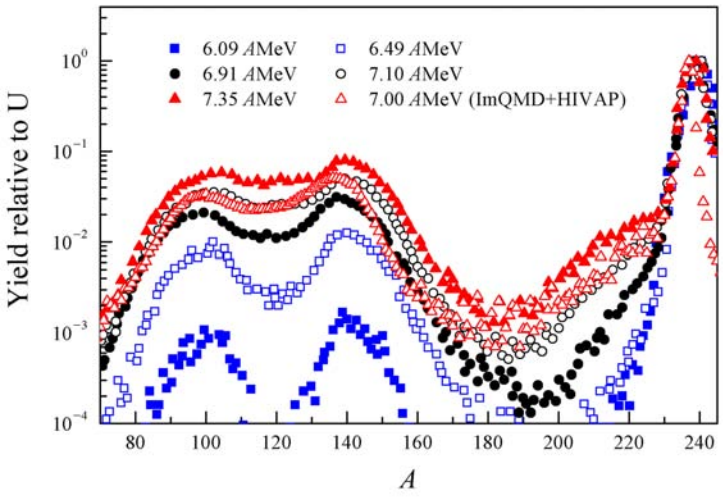

Fig. 10 (color online) The mass distribution of the products of reaction ^{238}U+^{238}U. The experimental data are taken from Ref. [16].

around Pb; (4) In the region below $A \approx 190$, a double hump distribution is observed. This is clearly due to the fission of actinide and transuranic nuclei, which results in the superposition of symmetric and asymmetric fission.

4 Summary

In this paper within the ImQMD model combining with the statistical-evaporation model, the large mass transfer reactions, like ^{238}U+^{238}U have been studied. The charge and mass distributions of transiently formed primary fragments are investigated by the ImQMD model and de-excitation processes of those primary fragments are described by the statistical decay model. The mass distribution of the final products in ^{238}U+^{238}U collisions is obtained and compared with the recent experimental data. It is found that the behavior of the calculated mass distribution at 7.0 *A*MeV is generally in agreement with the data at the incident energy 7.10 *A*MeV. In order to manifest the large mass transfer reaction to be very benefit for the production of neutron-rich transfermium isotopes, we compare three reactions of ^{238}U, ^{136}Xe, and ^{48}Ca with curium target. It has been shown that the cross sections for formation of new neutron-rich isotopes of transfermium elements in the transfer reaction of uranium beam with ^{248}Cm target are larger by several orders of magnitude as compared with that in the fusion reactions of ^{136}Xe, and ^{48}Ca with curium target. These results indicate that the large mass transfer reaction is very benefit for the production of transfermium elements (SH elements).

References:

[1] HOFMANN S, MÜNZENBERG G. Rev Mod Phys, 2000, **72**: 733.

[2] MORITA K, MORIMOTOK，KAJI D，*et al*. J Phys Soc Jpn, 2007, **76**: 043201.

[3] OGANESSIAN Y T, ABDULLIN F S, BAILEY P D, *et al*. Phys Rev Lett, 2010, **104**: 142502.

[4] OGANESSIAN Y T, UTYONKOV V. K, LOBANOV Y V, *et al*. Phys Rev C, 2006, **74**: 044602.

[5] ZAGREBAEV V I , GREINER W. Phys Rev C, 2008, **78**: 034610.

[6] WANG N, LI Z, WU Z. Mod Phys Lett A, 2005, **20**: 2619; TIAN J, WU X, ZHAO K, *et al*. Phys Rev C, 2008, **77**: 064603; ZHAO K, WU X, LI Z. Phys Rev C, 2009, **80**: 054607.

[7] COLABEK C, SIMENEL C. Phys Rev Lett, 2009, **103**: 042701; GOLABEK C. Int J Mod Phys E, 2009, **17**: 2235.

[8] ZAGREBAEV V I, GREIONER W. Phys Rev C, 2006, **73**: 031602; 2008, **78**: 034610; 2010, **81**: 044608; 2011, **83**: 044618.

[9] FENG Z, JIN G, LI J. Phys Rev C, 2009, **80**: 067601.

[10] ZAGREBAEV V I, GREIONER W. Phys Rev C,2011, **83**: 044618.

[11] ITKIS M G, AY ˜OTO˜ J, BEGHINO,*et al*. Nuc Phys A, 2004, **734**: 136.

[12] ZAGREBAEV V I , GREINER W. J Phys G, 2005, **31**: 825.

[13] NEUZIL E F, FAIRHALLN A W. Phys Rev, 1963, **129**: 2705.

[14] BENLLIURE J, GREWE A, JONG M D, *et al*. Nucl Phys A, 1998, **628**: 458.

[15] SCHMIDT K H, STEINHÄUSER S, BÖCKSTIEGEL C, *et al*. Nucl Phys A, 2000, **665**: 221.

[16] GORODISSKIY D M, MULGIN S I, OKOLOVICH V N, *et al*. Phys Lett B, 2002, **548**: 45.

[17] IAEA Library Cataloguing in Publication Data, Fission Product Yield Data for the Transmutation of Minor Actinide Nuclear Waste, international Atomic Energy Agency, Vienna, (ISBN 92-0-115306-6), 2008.

[18] GLENDENIN L E, GINDLER J E, AKMAD I, *et al*. Phys Rev C, 1980, **22**: 152.

[19] SCHMITT H W, KIKER W E, WILLIAMS C W. Phys Rev B, 1965, **137**: 837.

[20] JOHN W, HULET E K, LOUGHEED R W, *et al*. Phys Rev Lett, 1971, **27**: 45.

[21] GOLABEK C, VILLARI A C C, HEINZ S, *et al*. Int J Mod Phys E, 2008, **17**: 2235.

原子核的大质量转移反应和丰中子超重核的产生

吴锡真[1, 1)]，赵 凯[1]，李祝霞[1]，王 宁[2]，田俊龙[3]，张英逊[1]

(1. 中国原子能科学研究院，北京 102413；
2. 广西师范大学，广西 桂林 541004；
3. 安阳师范学院，河南 安阳 455000)

摘要： 迄今为止，人们合成的超重核都是缺中子的，无论是熔合-裂变反应还是碎化过程都无法使产物达到周期表的“东北区域”。而重核之间(如U核之间)的近垒大质量转移反应则可能是目前生成丰中子超重核和达到未知丰中子重核区域的唯一途径。在改进的量子分子动力学(ImQMD)模型结合统计模型框架内，研究了U+U等反应体系的大质量转移反应，计算了反应产生的初生态碎片的质量和电荷分布，并成功再现了产物的终态质量和电荷分布。通过比较3个反应 ^{136}Xe+^{248}Cm，^{48}Ca+^{248}Cm和^{238}U+^{248}Cm 产生的106号元素的截面大小，揭示了U+U等重核大质量转移反应对产生丰中子超重核是非常有利的。

关键词： 大质量转移反应；超重核；U+U反应；丰中子重核

收稿日期： 2012-10-29； **修改日期：** 2013-03-25

基金项目： 国家自然科学基金资助项目(11005022，11005155，10875031，10975095，10905021，91126010，11005003，U1230127)；国防基础科研计划资助项目(B0120110034)

1) E-mail: lizwux@ciae.ac.cn